

QA76  
D532  
CRL  
90/14

# Reconstructing and Visualizing Models of Neuronal Dendrites

Ingrid Carlbom<sup>1</sup>      Demetri Terzopoulos<sup>2</sup>  
Kristen M. Harris<sup>3</sup>

Digital Equipment Corporation  
Cambridge Research Lab

CRL 90/14

December 28, 1990

## Abstract

Neuroscientists have studied the relationship between nerve cell morphology and function for over a century. To pursue these studies, they need accurate three-dimensional models of nerve cells that facilitate detailed anatomical measurement and the identification of internal structures. Although serial transmission electron microscopy has been a source of such models since the mid 1960s, model reconstruction and analysis remain very time consuming. We have developed a new approach to reconstructing and visualizing 3D nerve cell models from serial microscopy. An interactive system exploits recent computer graphics and computer vision techniques to significantly reduce the time required to build such models. The key ingredients of the system are a digital "blink comparator" for section registration, "snakes," or active deformable contours, for semi-automated cell segmentation, and voxel-based techniques for 3D reconstruction and visualization of complex cell volumes with internal structures.

Keywords: scientific visualization, 3D reconstruction, image registration, image segmentation, contour tracking, snakes, volume rendering, dendrites, dendritic spines

AVS is a trademark of Stardent, Inc.

ICAR is a trademark of ISG Technologies, Inc.

VoxelView is a trademark of VitalImages, Inc.

NPL/RESEARCH LIBRARY  
BUILDING 734  
FBI BOX 10750  
FALLEN, CA 94530-0875

©Digital Equipment Corporation 1991. All rights reserved.

<sup>1</sup>DEC Cambridge Research Lab

<sup>2</sup>University of Toronto

<sup>3</sup>Children's Hospital



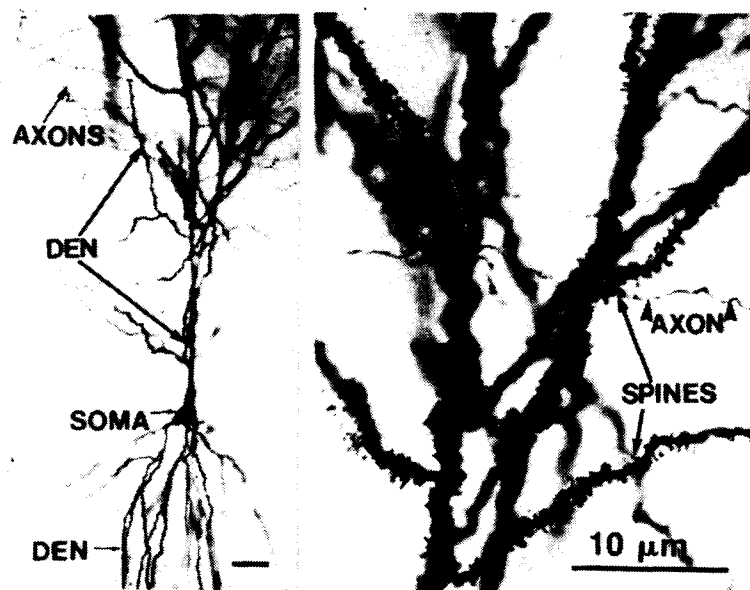


Figure 1: A hippocampal pyramidal cell with the soma and the dendrites (den) visible. The axons are from other hippocampal cells that form synapses with these dendrites. At higher magnification the dendritic spines are seen protruding from the dendrite. Bars =  $10\mu\text{m}$ . (Reproduced from (Harris et al., 1980) with permission from the publisher.)

## 1 Introduction

Neuroscientists search for links between neuronal dendritic morphology and behavior, and morphology and disease by studying the relationship between the morphology and function. Detailed morphological studies require accurate three-dimensional models of nerve cells that facilitate anatomical measurement and identification of internal structures. Neuronal dendrites and their protruding dendritic spines can be seen with a light microscope (Figure 1), but the resolution is insufficient for detailed anatomical measurement and the internal structures are not visible. To date, the only method available for detailed measurement and study of internal cell structure is through 3D reconstructions from serial electron microscopy, or serial EM (Figure 2) (Harris and Stevens, 1988; Harris and Stevens, 1989; Stevens and Trogadis, 1984; Wilson et al., 1987).

Reconstructions from serial EM have been produced almost since the invention of the electron microscope. Initially, the reconstructions were purely manual, but over the years they have relied increasingly on computers. Even with current computer-assisted techniques, the reconstruction of a  $5\mu\text{m}$  dendritic segment with all of its spines and synapses, along with the quantitative analysis of the reconstructed model, can take up to three months of work. By contrast, the tissue preparation and EM photography take only about two days! It is remarkable that so many neuronal reconstructions have been made because "... the incredible investment in time and energy necessary to reconstruct cells is nothing short of heroic" (Stevens and Trogadis, 1984).

We present a new interactive approach to reconstructing and visualizing 3D nerve cell models from serial microscopy, and describe an interactive system which exploits recent computer graphics and computer vision techniques to reduce significantly the time required to build such models. After presenting a more detailed review of the relevant neurophysiological motivation for our work and its relationship to prior efforts, we describe the key components of our approach to reconstruction and analysis of neuronal dendrites. Our prototype system currently features a digital “blink comparator” for section registration, “snakes,” or active deformable contours, for semi-automated cell segmentation, and voxel-based techniques for 3D reconstruction and visualization of the 3D morphology of dendrites along with their internal structures.

## 1.1 Background

A nerve cell, or neuron, has four constituent parts: the cell body (soma), the dendrites, the axon, and the presynaptic terminal of the axon (Kandel and Schwartz, 1985). The soma is the metabolic center of the cell, the dendrites are the receiving units, the axon is the conducting unit, and the presynaptic terminals are the transmitting units. The areas of contact between the presynaptic axonal terminals of one cell and the dendrites of another cell are called the synapses. Most synapses are located at the end of protrusions on the dendrites, called the dendritic spines (see Figure 1).

In humans, the dendritic spines are lost or change shape both with aging (Feldman and Dowd, 1975) and with diseases that affect the nervous system, such as dementia (Catala et al., 1988), brain tumors (Spacek, 1987), Down’s syndrome (Marin-Padilla, 1976), epilepsy (Scheibel, Crandall and Scheibel, 1940), Huntington’s disease (Graveland, Williams and DiFiglia, 1985), and alcoholism (Ferrer et al., 1986). Detailed anatomical descriptions of the synapses and dendritic spines will provide new understanding about their function, thus improving opportunities for understanding the underlying causes and effects of these diseases.

The dendritic spine is positioned so that changes in its morphology could modulate the transfer of information from the synapse to the dendrite (Brown et al., 1988a; Wickens, 1988). Direct physiological study of the relationship between dendritic spine morphology and function has been impossible because of their small size. Several simulations with theoretical models have shown, however, that small changes in morphology could change the biophysical properties of the spines (Rall, 1974; Crick, 1982). Several laboratory studies have shown that dendritic spines change shape during maturation, following experience, and in response to direct physiological stimulation of the presynaptic axon. Repeated, or “tetanic,” stimulation causes an enhanced synaptic efficacy, which is referred to as long-term potentiation (LTP), a leading candidate for a synaptic explanation of behavioral learning (Brown et al., 1988b). Anatomical analyses of stimulated dendrites have revealed swollen spines and changes in the size of synapses (for a review see (Harris, Jensen and Tsao, 1989)). Thus, a change in morphology might contribute to, or represent, the increase in synaptic efficacy which is observed after stimulation.

Research has also shown that the cytoskeleton and the organelles internal to the neuron, such as neurofilaments, microtubules, mitochondria, and smooth endoplasmic

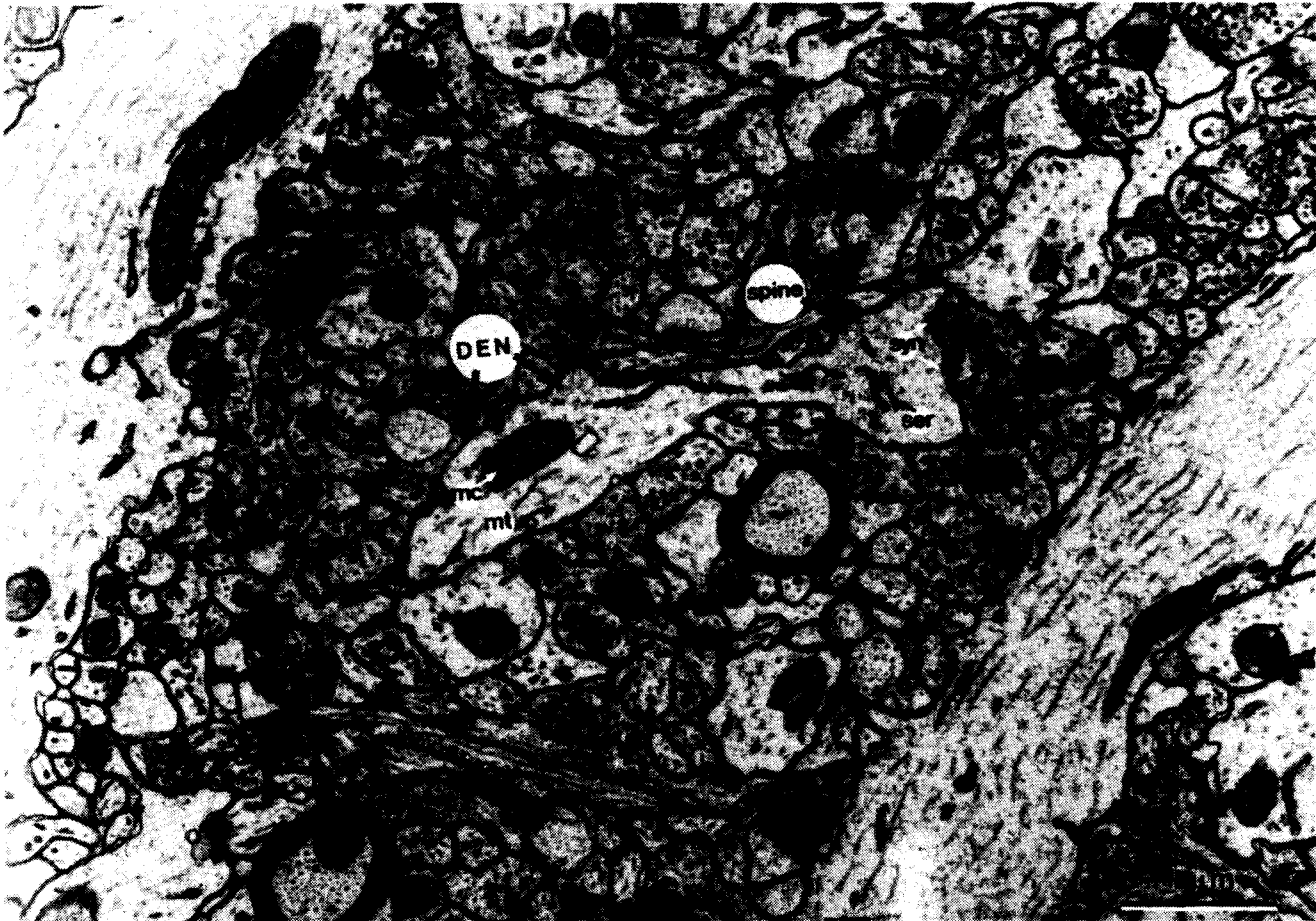


Figure 2: An EM photomicrograph from a section of a rat hippocampus. The dendrite (den) is located in the center, and a large spine is protruding from its right side. The mitochondrion (mc), microtubules (mt), some smooth endoplasmic reticulum (ser), and the synapse (syn) are indicated. Bar =  $1\mu m$ .

reticulum (see Figure 2) may control the shape of the nerve cell (Harris and Stevens, 1988; Harris and Stevens, 1989). The challenge is to find links between neuronal morphology and physiological function in the normal and diseased brain (Brown et al., 1988a).

## 1.2 Previous work

**Registration and Reconstruction:** Early EM reconstruction techniques were entirely manual (Stevens et al., 1980). A photograph from an electron microscope was illuminated from below and the outline of the structures of interest were traced on a sheet of acetate positioned on top of the print. Next a photograph of an adjoining section was illuminated and aligned with the trace from the previous section, and its structures were then traced on a new sheet of acetate. This process was repeated for all sections. The thickness of the acetate and the magnification were chosen so

that a fairly accurate model would result by inserting a number of blank sheets of acetate between each trace. Finally, an artist would produce a 2D illustration of the 3D model.

Over the years, reconstruction from serial EM has become increasingly computer assisted. In a system developed by Stevens *et al.* (1980; 1984), the EM negatives are first rephotographed onto a 35mm filmstrip. Next, the filmstrip is mounted on a film transport, which in turn is mounted on a stage driven by two computer-controlled stepping motors. The first image is digitized and stored in image memory. The second image is continually digitized while the user moves the film transport, and a video switcher alternately displays the stored and "live" images on a graphics screen at a frequency of about 4 Hz. There is an illusion of movement when the images are misaligned, and the movement is reduced as they are brought into alignment. When the motion is minimized between the two images or features of interest, the second image is stored. Next, serial sections two and three are aligned, followed by pairwise alignment of the remaining sections. Once the images are aligned, the features or boundaries of interest are traced manually using a bitpad. The traces can be displayed as a set of contours, as contours with the hidden lines removed, or tessellated to form a surface which can be displayed as a solid object (Harris and Stevens, 1989).

Using motion to compare photographs of the same or similar objects is not a new idea. Astronomers have used *blink comparators* since early this century to study astronomical plates (Crowell, 1990). A blink comparator holds two plates of the same part of the sky, and alternately displays them to the user. Stationary objects such as stars remain fixed, but objects such as comets or planets appear to move.

The problem of image alignment appears in many disciplines. Cartographers need to align aerial photographs, and in robot vision much effort is devoted to registration of stereo pairs and temporal image sequences (Horn, 1986). In both these disciplines, the images are different views of the *same* object, and in robot vision one can often assume that, at least locally, images are only misaligned translationally. The alignment of neural sections, however, is a considerably more difficult problem because the EM images are misaligned both translationally and rotationally and there is generally a large discrepancy between consecutive images. The latter is due both to the integration over the thickness of the section in the EM photographic process and to distortions of the tissue by its preparation and by the EM process.

Giertsen *et al.* (1990) propose a method to automatically align electron micrographs. They manually trace the membrane and internal substructures of a pancreatic cell in serial sections and specify connectivity relations among successive contours. Using contour shape features (centroids and mean radii), they determine linear transformations between successive contours and refine the alignment using residuals between the original and smoothed data. Aligned contours are tessellated and rendered as polygonal surfaces.

**Segmentation:** Many techniques have been developed for 3D image segmentation. One of the simplest techniques, intensity thresholding, has been used by (Drebin, Carpenter and Hanrahan, 1988) and (Hohne *et al.*, 1989) and works relatively well for separating soft and hard tissue in MR and CT scans. Surface normals are needed

for high-quality rendering, and they may be computed using 3D generalizations of 2D edge detectors; e.g., the Zucker-Hummel operator (Hohne et al., 1989). When the 3D volume cannot be segmented by simply looking at single intensity values, a larger voxel neighborhood can be used, by applying a 3D generalization of the Marr-Hildreth operator (Hohne et al., 1988; Hohne et al., 1989). Other 3D generalizations of edge detectors have also been used for segmentation (Liu, 1977; Zucker and Hummel, 1981; Morgenthaler and Rosenfeld, 1981).

Another technique for constructing polygonal representations of constant density surfaces from volumetric data is *marching cubes* (Lorensen and Cline, 1987). The data is assumed to be defined on a 3D lattice, and an iso-surface is approximated by finding all intersections between the iso-surface and the edges of the lattice. The technique dictates how to fill in the surface between the edges of a cube for each of the 14 different types of intersections that can occur between the surface and a cube in the lattice. The gradients are determined at each corner of the cube, and the surface is rendered using the gradients to estimate the surface normal.

Unfortunately, because of the complexity of EM images of neuronal tissue (see Figure 2), straightforward segmentation using any of the aforementioned techniques does not appear promising for 3D reconstruction of dendritic models. Therefore, we aim at introducing a higher level of automation into the section-by-section manual tracing methodology currently practiced by neuroscientists. A recently proposed model-based image feature localization and tracking technique known as *snakes* (Kass, Witkin and Terzopoulos, 1987) is well suited to this goal. This interactive technique is consistent with the manual tracing methods, but is considerably faster and more powerful.

The ability of snakes to conform to complex biological shapes such as cells and to track their nonrigid deformations across image sequences makes them attractive tools for biomedical image analysis. In (Leymarie, 1990), snakes are used to track living cells moving on a planar surface. Assuming modest interframe motion, snakes can exploit frame-to-frame coherence to track the moving cell and also follow the deformations which occur as the cell moves. Ayache *et al.* (1989) use snakes to find edges in cross sections of MR data. The user draws an approximate contour around the region of interest and the snake deforms to fit the regions more accurately. Once the snake has reached an equilibrium, it is used as a starting point for the next cross section. A 3D model is built from the the resulting set of contours using Delauney triangulation (Boissonnat, 1988). Variations on snakes based on B-splines have been applied to the segmentation of 3D CT and MR data (Leitner et al., 1990).

**Visualization:** Volume visualization is an area in computer graphics that has received a great deal of attention in recent years (Upson, 1989). Much work has been devoted to high-quality rendering of CT, PET, and MR data (Drebin, Carpenter and Hanrahan, 1988; Levoy, 1990) and seismic data (Sabella, 1988; Wolphe, Jr. and Liu, 1988). Specialized software and hardware has been developed to facilitate real-time manipulation of both medical data (Meagher, 1982; Meagher, 1984) and seismic data (Chakravarty, Nichol and Ono, 1986). More recently, general-purpose software for volume rendering has become available. Examples are ISG Technologies' ICAR System (Stevens and Trogadis, 1990), Stardent's AVS system (Upson et al., 1989) and VitalImages' VoxelView system (VitalImages, Inc., 1990). In our work, we use the

VoxelView system on a Silicon Graphics workstation to visualize the 3D reconstructed dendrites.

## 2 Reconstruction of Neuronal Dendrites

### 2.1 Data Acquisition

Using routine tissue processing, a slice ( $400\mu\text{m}$  thick) of well-preserved hippocampus was obtained from the brain of a male rat, and the slice was embedded in epoxy resin. The slice was further sectioned with an ultramicrotome, at an average section thickness of about  $0.06\mu\text{m}$ . (The dendritic segment used in this paper is dendrite number 24 of reference (Harris and Stevens, 1989)). Each section was photographed at 10,000 times magnification in a JEOL 100B transmission electron microscope and printed on 8x10 inch photographic paper (see Figure 2).

The EM photomicrographs were digitized on an ECRM Autokon flat-bed laser scanner capable of digitizing reflection copy images at a wide range of resolutions (Ulichney, 1982). The scanner has a fixed spot size and the intensity can be quantized at one or eight bits/pixel. We digitized the images at a resolution of  $2560\times 1983$  pixels, approximately twice the sampling rate of the smallest features of interest, and with eight bits of intensity per pixel. The images were low-pass filtered and subsampled to a size of  $640\times 496$  pixels.

### 2.2 Image Registration

We chose a manual approach to image registration for two reasons. First, the automatic alignment of successive EM images is a very difficult problem; because the images are displaced both translationally and rotationally and usually there is a large disparity between consecutive images. Second, even if an automated solution can be found, user intervention will be necessary when the tissue has been distorted during preparation; for example, when a section has a fold.

We have implemented an interactive digital blink comparator. One image is held stationary and the user translates and rotates the other image while the stationary and moving images are alternately shown on a graphics screen. The user can translate the image in the x- and y-directions and can rotate the image about its center by using a three-button mouse, each button controlling one type of motion. The user moves the image until the motion between the two images is minimized and the images are aligned. By using double buffering and by pre-computing x- and y-components of the composite transformation, we obtain comparisons at a frequency of about 1 Hz for a  $640\times 496$  pixel image on a Silicon Graphics 4D/220GTX using one of the R-3000 processors. We found this frequency adequate to obtain good alignment, although a higher speed would be desirable.

When all images are aligned by pairs, we find the composite transformation for each image relative to the first image in the EM series and resample the images using a spatially varying digital shift filter. This finite impulse response (FIR) filter is

designed with a conventional windowing technique (Oppenheim and Schafer, 1975). The resulting aligned images are input to the segmentation processes described in the next section.

## 2.3 Extracting Models from Electron Micrographs

The extraction of neuronal dendrites from a set of aligned EM images reduces to three subproblems: (i) the localization of dendritic profiles in digital micrographs, (ii) the segmentation of the interiors of dendrites bounded by profiles, and (iii) the identification of profiles of the same dendrite across serial micrographs. The density and geometric complexity of neuronal features in micrographs make the first and third subproblems especially difficult to automate fully.

We take a semi-automatic approach which exploits recently developed physically-based vision techniques for interactively localizing and tracking extended features in images. We employ a variant of snakes, the interactive deformable contour models introduced in (Kass, Witkin and Terzopoulos, 1987). Snakes provide significant assistance to the user in accurately locating the membranes that bound the dendrites in EM images. Using a mouse, the user quickly traces a contour which approximates the dendrite boundary, then starts a dynamic simulation that enables the contour to locate and conform to the true membrane boundary. Where necessary, the user may guide the contour by applying to it simulated forces using the mouse. Through minimal user intervention, snakes quickly produce accurate dendritic profiles in the form of complete, closed contours that facilitate the segmentation of dendritic interiors. Finally, with some guidance, snakes are able to exploit the coherence between serial micrographs to quickly extract a sequence of profiles of the same dendrite.

### 2.3.1 Deformable Contour Models

A snake can be thought of as a dynamic deformable contour in the  $x$ - $y$  image plane. We define a discrete deformable contour as a set of  $n$  nodes indexed by  $i = 1, \dots, n$ , with time varying positions  $\mathbf{x}_i(t) = [x_i(t), y_i(t)]'$ . The behavior of an interactive deformable contour is governed by the first-order dynamic system of equations

$$\gamma \frac{d\mathbf{x}_i}{dt} + \boldsymbol{\alpha}_i + \boldsymbol{\beta}_i = \mathbf{f}_i; \quad i = 1, \dots, n, \quad (1)$$

where  $\gamma$  is a velocity-dependent damping constant,  $\boldsymbol{\alpha}_i(t)$  are “compression” forces which make the snake act like a series of unilateral springs that resist compression,  $\boldsymbol{\beta}_i(t)$  are “rigidity” forces which make the snake act like a thin wire that resists bending, and  $\mathbf{f}_i(t)$  are forces in the image plane applied to the contour.

Let  $l_i$  be the given reference length of the spring connecting node  $i$  to node  $i + 1$  and let  $\mathbf{r}_i(t) = \mathbf{x}_{i+1} - \mathbf{x}_i$  be the separation of the nodes. Given the deformation  $e_i(t) = \|\mathbf{r}_i\| - l_i$ , we define

$$\boldsymbol{\alpha}_i = \frac{a_i e_i}{\|\mathbf{r}_i\|} \mathbf{r}_i - \frac{a_{i-1} e_{i-1}}{\|\mathbf{r}_{i-1}\|} \mathbf{r}_{i-1}. \quad (2)$$

To obtain contours that can stretch arbitrarily but resist shrinking past a prespecified amount, we set

$$a_i(t) = \begin{cases} a & \text{if } e_i < 0, \\ 0 & \text{otherwise,} \end{cases} \quad (3)$$

so that each spring resists compression with constant  $a$  only when its actual length  $\|\mathbf{r}_i\|$  is less than  $l_i$ . To give the contours some rigidity, we introduce the variables  $b_i$  and define rigidity forces

$$\begin{aligned} \beta_i = & b_{i+1}(\mathbf{x}_{i+2} - 2\mathbf{x}_{i+1} + \mathbf{x}_i) - 2b_i(\mathbf{x}_{i+1} - 2\mathbf{x}_i + \mathbf{x}_{i-1}) \\ & + b_{i-1}(\mathbf{x}_i - 2\mathbf{x}_{i-1} + \mathbf{x}_{i-2}). \end{aligned} \quad (4)$$

Note that in the absence of external forces, if the nodes are separated more than  $l_i$ , are equally spaced, and lie on a straight line,  $\alpha_i$  and  $\beta_i$  vanish and the contour will be at equilibrium. Compression and rigidity are locally adjustable through the  $a_i$  and  $b_i$  variables. In particular, by setting  $a_i = b_i = 0$ , we are able to break a long deformable contour into several shorter contours on an image.

To simulate the deformable contour we integrate the system of ordinary differential equations (1) forward through time using a semi-implicit Euler procedure (Press et al., 1986). Applying the forward finite difference approximation  $d\mathbf{x}_i/dt \approx (\mathbf{x}_i^{t+\Delta t} - \mathbf{x}_i^t)/\Delta t$  to (1) and collecting linear terms in the  $\mathbf{x}_i$  on the left yields the pentadiagonal system of algebraic equations

$$\frac{\gamma}{\Delta t} \mathbf{x}_i^{t+\Delta t} + \beta_i^{t+\Delta t} = \frac{\gamma}{\Delta t} \mathbf{x}_i^t - \alpha_i^t + \mathbf{f}_i^t \quad (5)$$

for the subsequent node positions  $\mathbf{x}_i^{t+\Delta t}$  in terms of the current positions  $\mathbf{x}_i^t$ . Since the system has a constant coefficient matrix, we factorize it only once at the beginning of the deformable contour simulation using a direct LDU factorization method and then efficiently resolve with different right-hand sides at each time step (see (Terzopoulos, 1987) for details).

After each simulation time step we draw lines between the new node positions  $\mathbf{x}_i^{t+\Delta t}$  to display the deformable contour as a dynamic curve in the image plane.

### 2.3.2 Image Segmentation using Deformable Contours

The deformable contour is responsive to an image force field which influences the contour's shape and motion. It is convenient to express the force field as the gradient of a potential function  $P_{I_s}(x, y)$  computed from the image  $I_s(x, y)$  of EM section  $s$ :

$$\mathbf{f}_i = \nabla P_{I_s}(\mathbf{x}_i), \quad (6)$$

where  $\nabla = [\partial/\partial x, \partial/\partial y]^t$ . By simulating (1) with (6), the ravines (extended local minima) of  $P_{I_s}$  act as attractors to deformable contours. The contours "slide downhill" and stabilize at the bottoms of the nearest ravines.

In the present application, we are interested in the localization of cell membranes, which appear dark in positive micrographs. We therefore convert  $I_s(x, y)$  into a 2D potential function whose ravines coincide with dark cell membranes:

$$P_{I_s}(x, y) = G_\sigma * I_s(x, y), \quad (7)$$

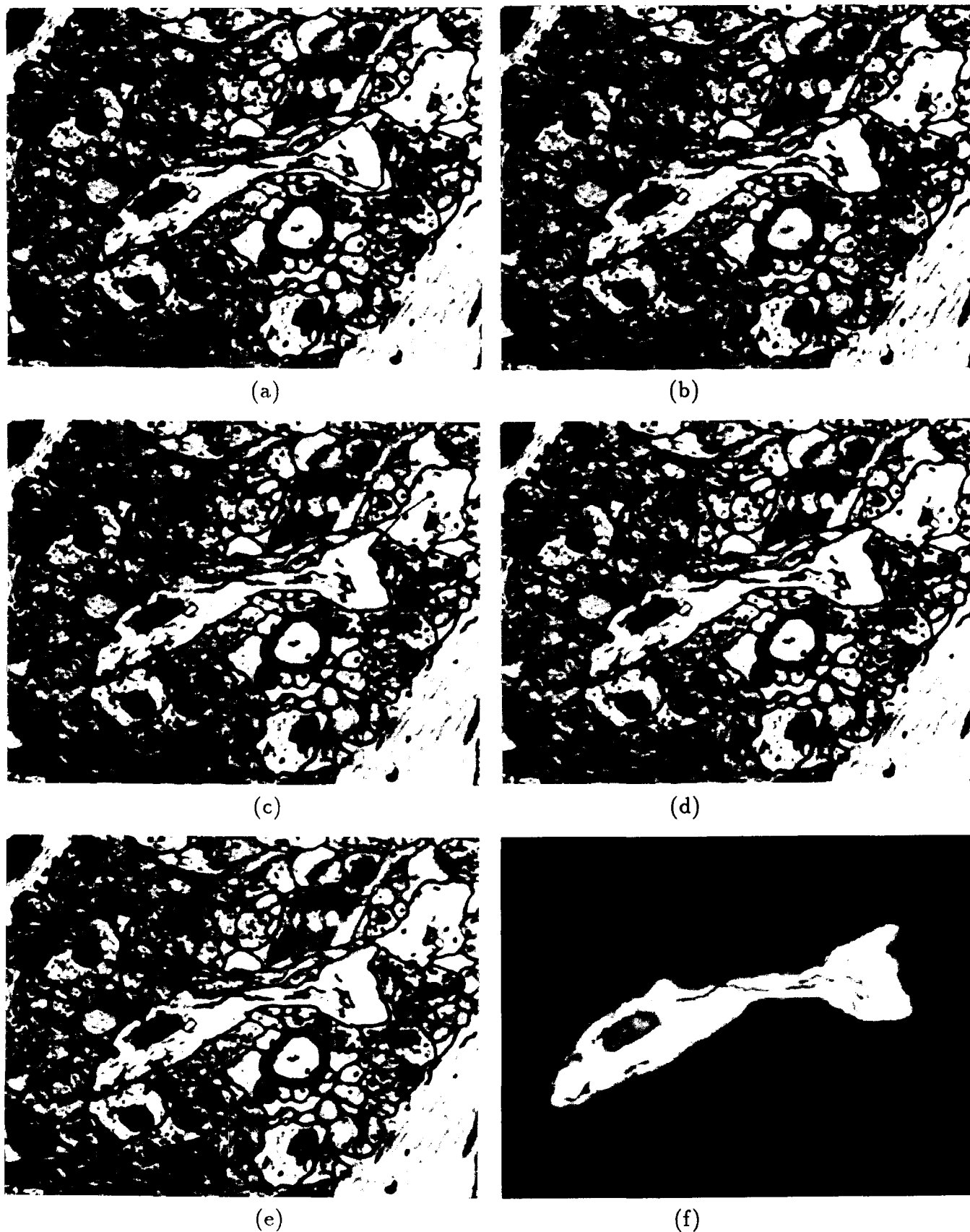


Figure 3: Cell segmentation using a deformable contour (see text). (a) Initial sketched contour. (b) Initial equilibrium position. (c)–(d) Manipulating the contour with interactive springs (green lines) and constraints (blue lines). (e) Final profile. (f) Segmented cell.



where  $G_\sigma*$  denotes convolution with a 2D Gaussian smoothing filter of width  $\sigma$ . The filter broadens the ravines of  $P_I$ , so that they attract the contours from some distance away.

In practice,  $I_s$  is not a continuous function, but a digital image. Therefore, we first convolve the image with a discrete smoothing kernel, then compute (6) by bilinearly interpolating the smoothed image gradients evaluated at the four pixels surrounding  $\mathbf{x}_i$ . The user can set the degree of smoothing  $\sigma$  and select the display of image  $I_s$ , or potential functions  $P_{I_s}$ , through a menu-driven interface.

The user initializes a closed deformable contour by quickly sketching with a mouse an approximate trace around the dark membrane of a dendrite of interest. Figure 3(a) shows an initial deformable contour sketched near a cell membrane (nodes are created automatically so that they are spaced about one pixel apart, and an additional spring is inserted between the first and last nodes to close the contour). The user then initiates the snake simulation (5). In a few simulation time steps the deformable contour equilibrates at the bottom of the nearest ravine in  $P_{I_s}$  (Figure 3(b)). By interacting with the contour (see below), the user can help it quickly localize the membrane ravine conform to its shape to produce an accurate profile of the dendrite (Figure 3(e)).

Because the dendritic profile is a closed continuous contour, it is easy to segment the interior of the cell from the rest of the image. We accomplish the segmentation by applying a standard region-fill algorithm (Foley et al., 1990) which starts from a seed point inside the profile and sequentially accesses the pixels of  $I_s$  that are bounded by the profile. Figure 3(f) shows the cell segmented from the dendritic profile of Figure 3(e).

### 2.3.3 User and Constraint Forces

Often the user will sketch an initial trace which deviates too much from the membrane ravine to descend into the ravine properly. This is the case for the initial contour in Figure 3(a) which reaches the equilibrium configuration shown in Figure 3(b). As can be seen, the deformable contour may fall prey to nearby dark features inside the cell (or to nearby features of neighboring cells) which act as false attractors. In such a case, the user may apply interactive simulated forces  $\mathbf{f}_i^m(t)$  by using the mouse to guide deformable contour towards the ravine of interest as it is stabilizing (see (Kass, Witkin and Terzopoulos, 1987) for details about user forces). A useful force is the interactive spring

$$\mathbf{f}_i^m = \begin{cases} \mathbf{x}_i - \mathbf{m}(t) & \text{if } \|\mathbf{x}_i - \mathbf{m}(t)\| \text{ is minimal for node } i, \\ 0 & \text{otherwise.} \end{cases} \quad (8)$$

which pulls the nearest node towards the time-varying mouse position  $\mathbf{m}(t)$  in the image plane. Figure 3(c) shows the effect of a user stretching the contour towards the right with an attached interactive spring (green line) from the mouse position (blue circle).

To localize a profile accurately, the user may want to constrain points on a deformable contour by attaching them with springs to selected anchor points on the

image. Such constraints prevent the deformable contour from straying far from these points, regardless of the image forces and the user’s other mouse manipulations. The mechanism for adding constraints is simply to fix  $\mathbf{m}(t) = \mathbf{a}_k$  in the spring force (8) to create an anchor point  $\mathbf{a}_k$  in the image. The constraining spring then applies a force  $\mathbf{f}_i^{\mathbf{a}_k}$ . Figure 3(d) illustrates a constraint spring (blue line) which pulls the contour back towards an anchor point on the cell membrane as the user tugs on the contour with an interactive spring (green line). Note the two constraints (blue dots) in the final profile contour in Figure 3(e).

Combining the three types of forces, we have

$$\mathbf{f}_i = c_I \nabla P_{I_s}(\mathbf{x}_i) + c_m \mathbf{f}_i^m + c_a \sum_k \mathbf{f}_i^{\mathbf{a}_k}, \quad (9)$$

where  $\sum_k$  is a summation over all the anchor constraints in force and where  $c_I$ ,  $c_m$ , and  $c_a$  are the strength factors of the image forces, user spring forces, and anchor spring forces.

### 2.3.4 Exploiting Coherence Across Serial Sections

Our interactive technique for extracting cell profiles from EM images benefits from the fact that snakes can exploit the coherence of profile positions and shapes across adjacent images. Often, the user need not reinitialize the deformable contours when progressing from image to image to extract adjacent profiles of a dendrite.

Once the deformable contours equilibrate into the membrane ravines in  $P_{I_s}$ , we replace this potential function with the potential function  $P_{I_{s\pm 1}}$  of an adjacent member of the image sequence. Continuing from their previous equilibrium positions, the contours automatically slide downhill to regain their equilibria in the new ravines, quickly localizing the new positions of the cell membranes in the adjacent image and conforming to their shapes.

This simple mechanism for exploiting image-to-image coherence works so long as the perturbation is small enough to maintain the deformable contours within the membrane ravines as we switch to adjacent images. Should part of a contour escape the ravine, however, the rest of the contour will usually pull it back into place due to the rigidity of the model. Nonetheless, deformable contour reinitializations are normally required when portions of the dendritic spines are no longer connected to the parent dendrite.

## 3 Visualizing Neuronal Dendrites

During image segmentation, the user can visualize what takes place in two graphics windows (Figure 4). The left window shows the current EM image overlaid with the deformable contour simulation. The right window displays a stack of dendritic profiles and their interiors. The user can also see the current contour with the (partial) model, thereby monitoring progress. The stacked set of contours and interiors can be rotated and viewed from different vantage points. When all the dendritic profiles

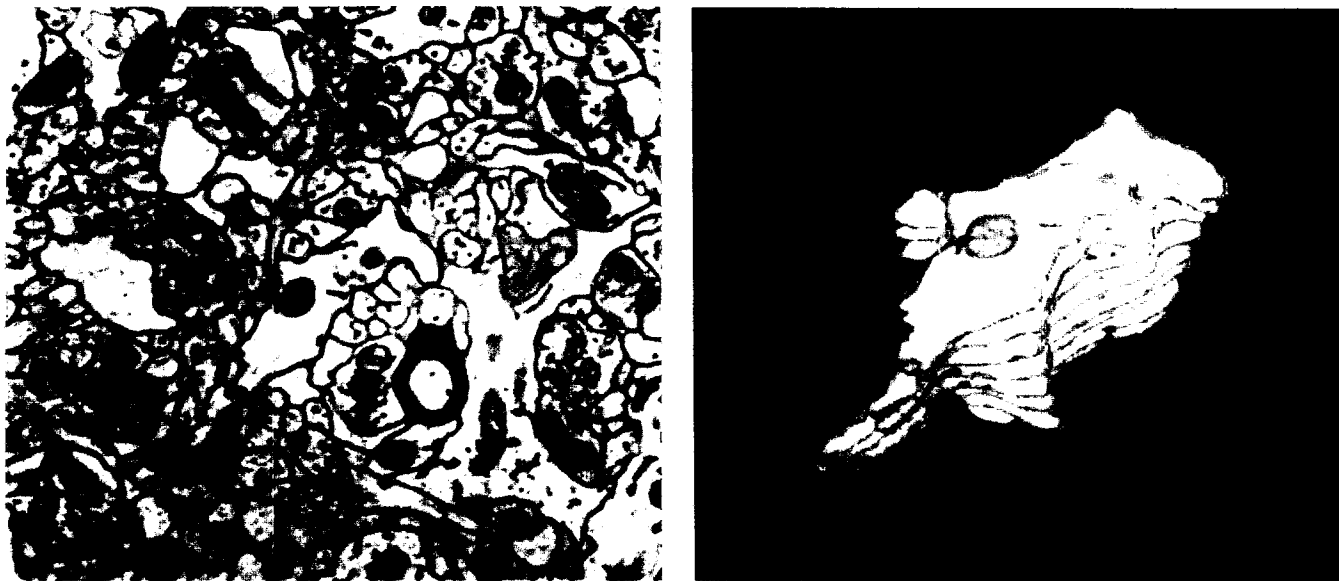


Figure 4: To the left, the current EM image with a deformable contour (snake); to the right, a stack of dendritic profiles and their interiors. The current snake is displayed in red.

have been found, we use the segmented dendritic interior to build a volumetric voxel model. We apply volume rendering techniques to visualize the volumetric model.

Volume rendering refers to the direct rendering of scalar data sampled in three dimensions. These techniques differ from traditional computer graphics techniques in that explicit surfaces need not be extracted from the data before display. Rather, the entire 3D volume of data is used for display. Yet, by displaying only the portions of the volume that have a given density or a high gradient, features and surfaces may be elicited without explicit representation (Foley et al., 1990).

We use the VoxelView system (VitalImages, Inc., 1990) to reconstruct a 3D volumetric model of a dendrite from the dendritic interiors that have been segmented from the serial sections. The segmented dendrite in each image is enclosed by a rectangular array of black pixels. The resulting arrays, or images, are stacked in order. The sizes of the rectangular arrays are chosen so that the stack yields a rectangular parallelepiped. Since the sampling rate is less in the stacking direction ( $z$ -direction) than in the  $x$ - and  $y$ -directions of the images, the VoxelView system linearly interpolates an additional number of sections. In the examples shown below, we have reconstructed 41 sections of a dendrite, and interpolated three sections between each pair of original sections to get approximately the correct proportions along the  $z$ -axis as we view all the sections.

By rapidly moving from one image to the next, we generate an interactive “movie” that enables us to follow certain features of interest through the dendrite. We can also slice the stack of images along planes perpendicular to the stacking direction, and along any arbitrary plane. Because of the tissue cutting direction, the dendrite is positioned obliquely in the image volume; therefore, we must cut the image volume



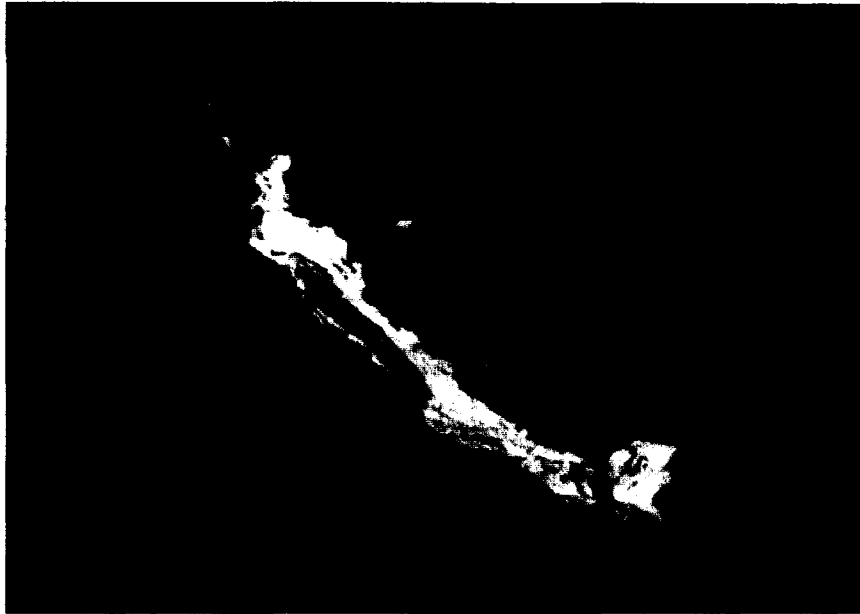


Figure 5: Oblique slice through model of a dendrite reconstructed from 41 serial sections. The mitochondrion can be seen extending through the length of the dendrite and some smooth endoplasmic reticulum is visible in the large spine.



Figure 6: Shaded model of the reconstructed dendrite.



obliquely to slice the dendrite lengthwise. One such oblique slice is shown in Figure 5, where we can see the shape and extent of the mitochondrion through the dendrite, and also some smooth endoplasmic reticulum.

By default, the volume is rendered without any shading; however, the user can specify the position of a light source and obtain a shaded view of the model. In Figure 6, we have rendered the dendrite model with shading. The shading helps accentuate the 3D shape of the dendrite. Other features of the VoxelView system that we find useful are the ability to tumble the model interactively and to make portions of the model transparent by adjusting the opacity values of the pixels (VitalImages, Inc., 1990).

By using a volumetric representation of the dendritic model, we can represent the 3D shape of the model with accuracy limited only by the original sampling of the EM images. Furthermore, we can visualize the cytoskeleton and the organelles interior to the dendrite.

## 4 Summary and Future Research

We have described a prototype system for the reconstruction and analysis of neuronal dendrites. Our goal is to reduce the effort required to reconstruct and analyze a complete dendrite from a few months to a few days. We are approaching this goal by exploiting three recently developed techniques for volume reconstruction: a digital blink comparator for EM section registration, snakes, or active energy-minimizing contours, for dendrite segmentation, and volume rendering to visualize both the overall morphology of 3D dendrites and their cytoskeleton and internal organelles.

Much work remains to be done to improve the reconstruction process. The digital blink comparator opens a way to use direct digitization from electron microscopes for serial microscopy. This would eliminate the need for rephotographing and digitizing EM photomicrographs, thus reducing the reconstruction time and eliminating distortions and quantization errors introduced by these processes. Direct digitization from an electron microscope has been used for single section studies, but has until now been impossible to use for serial microscopy, which requires section alignment (Stevens and Trogadis, 1984).

We need to provide (at least) a semi-automatic approach to image registration, with the user intervening only for optional fine-tuning. Currently, during manual alignment, we resample the image using nearest pixel sampling. It would be desirable, however, to allow subpixel alignment and resampling by using a spatially varying shift filter, but this is computationally prohibitive with our current equipment. Despite the sampling limitations, we have found the resulting alignments to be quite satisfactory.

We need to improve upon the snakes' behavior at spine branching points, to reduce the amount of user assistance required when dendritic spines are no longer connected to the parent dendrite.

We need to improve upon interslice interpolation to allow fractional section interpolation; that is, proper resampling of the volume to get accurate proportions in the x-, y-, and z-directions. Similarly, we need to provide better inter-pixel interpolation

at volume slicing and rendering in order to reduce aliasing without compromising image accuracy.

We have not yet begun to tackle anatomical analysis of the dendrites. We expect, however, that through (semi-)automated approaches for dendrite decomposition, anatomical measurements, and statistical analysis of these measurements, we can achieve reductions in analysis times similar to those that we are beginning to realize in the reconstruction phase.

When we have reached our goal, the time required to reconstruct and analyze neurons or parts of neurons will be reduced from a few months to a few days. It will then be possible to obtain a sufficiently large number of reconstructions to evaluate quantitatively the functional consequences that alterations in neuronal morphology have for both the normal and diseased brain.

## 5 Acknowledgments

The authors would like to thank Victor Vyssotsky, Director of Digital Equipment Corporation's Cambridge Research Lab, for his support of this research. This work has benefited from many discussions with Gudrun Klinker and Richard Szeliski, and from the use of image conversion software written by Richard Szeliski. We would like to thank Robert Ulichney and Victor Bahl for their help with the Autokon scanner. We also thank Dick Beane, Gudrun Klinker, and Richard Szeliski for reading and commenting on the manuscript. Ingrid Carlbom and Kristen Harris thank David Margulies at The Children's Hospital for having introduced us.

## References

- Ayache, N., Boissonnat, J. D., Brunet, E., Cohen, L., Chieze, J. P., Geiger, B., Monga, O., Rocchisani, J. M., and Sander, P. (1989). Building highly structured volume representations in 3D medical images. In *Proc. 3rd International Symposium on Computer Assisted Radiology, CAR'89*, pages 765–772, New York. Springer-Verlag.
- Boissonnat, J. D. (1988). Shape reconstruction from planar cross-sections. *Computer Vision, Graphics, and Image Processing*, 44:1–29.
- Brown, T. H., Chang, V. C., Ganong, A. H., Keenan, C. L., and Kelso, S. R. (1988a). Biophysical properties of dendrites and spines that may control the induction and expression of long-term synaptic potentiation. *Neurology and Neurobiology*, 35:201–264.
- Brown, T. H., Chapman, P. F., Kairiss, E. W., and Keenan, C. L. (1988b). Long-term synaptic potentiation. *Science*, 242:724–728.
- Catala, I., Ferrer, I., Galofre, E., and Fabreques, I. (1988). Decreased numbers of dendritic spines on cortical pyramidal neurons in dementia: A quantitative Golgi

- study on biopsy samples. *Human Neurobiology*, 6:255–259.
- Chakravarty, I., Nichol, B. G., and Ono, T. (1986). The integration of computer graphics and image processing techniques for the display and manipulation of geophysical data. In Kunii, T., editor, *Advanced Computer Graphics*, pages 318–333, Tokyo, Japan. Springer-Verlag.
- Crick, F. (1982). Do dendritic spines twitch? *Trends in Neuroscience*, 5:44–46.
- Croswell, K. (1990). The pursuit of Pluto. *American Heritage of Invention and Technology*, 5(3):50–57.
- Drebin, R. A., Carpenter, L., and Hanrahan, P. (1988). Volume rendering. *Computer Graphics*, 22(4):65–74.
- Feldman, M. L. and Dowd, C. (1975). Loss of dendritic spines in aging cerebral cortex. *Anatomy and Embryology*, 148:279–301.
- Ferrer, I., Fabreque, I., Rairiz, J., and Galofre, E. (1986). Decreased numbers of dendritic spines on cortical pyramidal neurons in human chronic alcoholism. *Neuroscience Letters*, 69:115–119.
- Foley, J. D., van Dam, A., Feiner, S. K., and Hughes, J. F. (1990). *Computer Graphics: Principles and Practice*. Addison-Wesley Publishing Company, Reading, MA.
- Giertsen, C., Halvorsen, A., and Flood, P. R. (1990). Graph-directed modelling from serial sections. *The Visual Computer*, 6(5):284–290.
- Graveland, G., Williams, R. S., and DiFiglia, M. (1985). Evidence for degenerative and regenerative changes in neostriatal spiny neurons in Huntington's disease. *Science*, 227:770–773.
- Harris, K. M., Cruce, W. L. R., Greenough, W. T., and Teyler, T. J. (1980). A Golgi impregnation technique for thin brain slices maintained in vitro. *Journal of Neuroscience Methods*, 2:363–371.
- Harris, K. M., Jensen, F. E., and Tsao, B. H. (1989). Ultrastructure, development, and plasticity of dendritic spine synapses in area CA1 of the rat hippocampus: Extending our vision with serial electron microscopy and three-dimensional analysis. *Neurology and Neurobiology*, 52:33–52.
- Harris, K. M. and Stevens, J. K. (1988). Dendritic spines of rat cerebellar Purkinje cells: Serial electron microscopy with reference to their biophysical characteristics. *The Journal of Neuroscience*, 8(12):4455–4469.
- Harris, K. M. and Stevens, J. K. (1989). Dendritic spines of CA1 pyramidal cells in the rat hippocampus: Serial electron microscopy with reference to their biophysical characteristics. *The Journal of Neuroscience*, 9(8):2982–2997.

- Hohne, K. H., Bomans, M., Pommert, A., Riemer, M., Schiers, C., Tiede, U., and Wiebecke, G. (1989). 3D visualization of tomographic volume data using the generalized voxel-model. In Upson, C., editor, *Proceedings of Volume Visualization Workshop*, pages 51–57, Chapel Hill, NC. Department of Computer Science, University of North Carolina.
- Hohne, K. H., Bomans, M., Pommert, A., Riemer, M., and Tiede, U. (1988). 3D segmentation and display of tomographic imagery. In *Proc. International Conference on Pattern Recognition*, pages 1271–1276, Rome, Italy. IEEE Computer Society Press.
- Horn, B. K. P. (1986). *Robot Vision*. MIT Press, Cambridge, Massachusetts.
- Kandel, E. R. and Schwartz, J. H. (1985). *Principles of Neural Science*. Elsevier Science Publishing Co., Inc., New York, NY.
- Kass, M., Witkin, A., and Terzopoulos, D. (1987). Snakes: Active contour models. *International Journal of Computer Vision*, 1(4):321–331.
- Leitner, F., Marque, I., LaVallee, S., and Cinquin, P. (1990). Dynamic segmentation: Finding the edge with differential equations and 'spline snakes'. Technical Report TIMB - TIM 3 - IMAG, Faculte de Medecine, 38700 La Tronche, France.
- Levoy, M. (1990). Efficient ray-tracing of volume data. *ACM Transactions on Graphics*, 9(3):245–261.
- Leymarie, F. (1990). Tracking and describing deformable objects using active contour models. Master's thesis, Computer Vision and Robotics Laboratory, McGill Research Centre for Intelligent Machines, McGill University, Montreal, QC, Canada.
- Liu, H. K. (1977). Two and three dimensional boundary detection. *Computer Graphics and Image Processing*, 6:123–134.
- Lorensen, W. E. and Cline, H. E. (1987). Marching cubes: A high resolution 3D surface construction algorithm. *Computer Graphics*, 21(4):163–169.
- Marin-Padilla, M. (1976). Pyramidal cell abnormalities in the motor cortex of a child with Down's syndrome: A Golgi study. *Journal of Computational Neurology*, 167:63–82.
- Meagher, D. (1982). Geometric modeling using octree encoding. *Computer Graphics and Image Processing*, 19:129–147.
- Meagher, D. (1984). Interactive solids processing for medical analysis and planning. In *Proceedings of National Computer Graphics Association, NCGA '84*.
- Morgenthaler, D. G. and Rosenfeld, A. (1981). Multidimensional edge detection by hypersurface fitting. *IEEE Transactions on Pattern Analysis and Machine Intelligence*, 3(4):482–486.

- Oppenheim, A. V. and Schaffer, R. W. (1975). *Digital Signal Processing*. Prentice Hall, Inc., Englewood Cliffs, New Jersey.
- Press, W. H., Flannery, B. P., Teukolsky, S. A., and Vetterling, W. T. (1986). *Numerical Recipes: The Art of Scientific Computing*. Cambridge University Press, Cambridge, England.
- Rall, W. (1974). Dendritic spines, synaptic potency, and neuronal plasticity. In Woody, C., Brown, K., Crow, T., and Knispel, J., editors, *Cellular Mechanisms Subservicing Changes in Neuronal Activity*, pages 13–21. Brain Information Service, Los Angeles, CA.
- Sabella, P. (1988). A rendering algorithm for visualizing 3D scalar fields. *Computer Graphics*, 22(4):51–58.
- Scheibel, M. E., Crandall, P. H., and Scheibel, A. B. (1940). The hippocampal-dentate complex in temporal lobe epilepsy. *Epilepsia*, 15:55–80.
- Spacek, J. (1987). Ultrastructural pathology of dendritic spines in epitemorous human cerebral cortex. *Acta Neuropathology*, 73:77–85.
- Stevens, J. K., Davis, T. L., Friedman, N., and Sterling, P. (1980). A systematic approach to reconstructing microcircuitry by electron microscopy of serial sections. *Brain Research Reviews*, 2:265–293.
- Stevens, J. K. and Trogadis, J. (1984). Computer-assisted reconstruction from serial electron micrographs: A tool for the systematic study of neuronal form and function. *Advances in Cellular Neurobiology*, 5:341–369.
- Stevens, J. K. and Trogadis, J. (1990). A systematic approach to 3D confocal microscopy: Application of volume investigation methods. *Journal of Microscopy*. In press.
- Terzopoulos, D. (1987). On matching deformable models to images: Direct and iterative solutions. In *Topical Meeting on Machine Vision*, pages 160–167, Washington, D.C. Optical Society of America.
- Ulichney, R. (1982). *Image Lab Picture Files, Internal Memo*. Digital Equipment Corporation, Maynard, MA.
- Upton, C., editor (1989). *Proceedings of the Chapel Hill Workshop on Volume Visualization*, Department of Computer Science, University of North Carolina, Chapel Hill, NC.
- Upton, C., Faulhaber Jr., T., Kamins, D., Laidlaw, D., Schlegel, D., Vroom, J., Gurwitz, R., and van Dam, A. (1989). The application visualization system: A computational environment for scientific visualization. *IEEE Computer Graphics and Applications*, 9(4):30–42.

- VitalImages, Inc. (1990). *VoxelView/PLUS 1.4, The interactive volume rendering system*. Fairfield, IA.
- Wickens, J. (1988). Electrically coupled but chemically isolated synapses: Dendritic spines and calcium in a rule for synaptic modification. *Progress in Neurobiology*, 31:507-528.
- Wilson, C. J., Murakami, F., Katsumaru, H., and Tsukahara, N. (1987). Dendritic and somatic appendages of identified rubrospinal neurons of the cat. *Neuroscience*, 22:113-130.
- Wolphe, Jr., R. H. and Liu, C. N. (1988). Interactive visualization of 3D seismic data: A volumetric method. *IEEE Computer Graphics and Applications*, 8(4):24-30.
- Zucker, S. W. and Hummel, R. A. (1981). A three-dimensional edge operator. *IEEE Transactions on Pattern Analysis and Machine Intelligence*, 3(3):324-331.